

# Coupling internal atomic states in a two-component Bose-Einstein condensate via an optical lattice: Extended Mott-superfluid transitions

Jonas Larson and Jani-Petri Martikainen  
 NORDITA, 106 91 Stockholm, Sweden  
 (Dated: February 6, 2020)

An ultracold gas of coupled two-component atoms in an optical lattice is studied. A systematic derivation of a Bose-Hubbard model is presented, and we explicitly demonstrate that the hopping coefficient amongst neighboring sites may be tuned between positive and negative values. This originates from the interplay between atomic kinetic, atomic internal and atom-atom interaction energies. As a consequence, the superfluid phase is divided into ferromagnetic and antiferromagnetic like states. Furthermore, also the Mott phase is separated into two distinguishable states. By means of the strong coupling expansion, we find the full phase diagram of the four different phases.

PACS numbers: 37.10.Jk,05.30.Jp,03.75.Mn,03.75.Lm

## I. INTRODUCTION

Ultracold atoms in optical lattices provides a test-ground of strongly interacting many-body systems. The advantages of these systems compared to corresponding models in condensed matter physics lie in the high controllability in terms of purity, parameters, state preparation, and state detection [1]. Since the seminal experiment by Bloch and co-workers, where the Mott-superfluid phase transition was first realized [2], numerous experimental achievements have been accomplished. For example, Anderson localization of matter waves [3], the Tonks gas characterized by strong atom-atom interaction [4] and the Mott phase of two fermionic compounds [5].

Systems composed of atoms with internal level structure, such as spinor gases, yield other interesting possibilities. It has been demonstrated that the additional internal degree of freedom give rise to novel phases and quantum phase transitions [6]. Experiments on spinor condensates include for example, coherent transport in optical lattices [7], spin-mixing [8], inherent spin tunneling [9] and symmetry breaking [10]. In these works, as for mixtures of atomic species in optical lattices [11], direct coupling between the internal states is not considered. Coupling between the internal atomic states may indeed render new phenomena. Krutitsky *et al.* studied a  $\Lambda$  configuration for the atoms, coupled by two optical lattices [12, 13]. They particularly showed that the Mott-superfluid phase transition may be of first order nature and that ferromagnetic and antiferromagnetic type of superfluid states can exist in such coupled models. Later in Ref. [14], Garcìa-Ripol and co-workers considered individual lattice configurations for internal (dressed) atomic states. Coupling between atoms in these two lattices was induced by atom collisions. In an earlier contribution [15], we demonstrated an inherent topological phase transition in fermionic systems originating from the interplay between internal and external atomic degrees of freedom rather than kinetic and atom-atom interaction energies as is normally the case for cold atoms in optical lattices.

In this paper we examine a gas of ultracold interacting

$\Lambda$ -atoms in an optical lattice. The two atomic transitions are driven by respectively one laser field rendering the optical lattice and another external laser lacking any spatial dependence in its mode profile. The largely detuned excited atomic level is adiabatically eliminated resulting in an effective coupled  $2 \times 2$  model. In the next Section we show that the spectrum of the single particle Hamiltonian possesses several interesting features, such as anomalous dispersions with multiple local minima. The many-body Hamiltonian is derived in Sec. III using an expansion of the atom field operators in the lowest band Wannier functions. The magnitudes of the Hamiltonian parameters, obtained from overlap integrals containing the numerically achieved Wannier functions, allow us to collect the significant terms. In the parameter regimes studied in this contribution, we end up with a Bose-Hubbard Hamiltonian. Utilizing the strong coupling expansion, we are able to find the system phase diagram in Sec. IV B. Opposite to the regular tight-binding Bose-Hubbard model, our system possesses four different phases: antiferromagnetic and ferromagnetic superfluid states and two Mott states characterized by different collective atomic population inversions. The effects of changing sign of the nearest neighbor hopping coefficient is addressed in Sec. V. We especially demonstrate that time-of-flight measurements would provide the information needed to distinguish between the two possibilities.

## II. SINGLE PARTICLE HAMILTONIAN

In order to obtain a many-body theory, we first consider properties of the corresponding single particle Hamiltonian. This enables us to systematically derive the many-body counterpart which includes atom-atom interaction in the next Section.

### A. The model system

We consider an ultracold three-level  $\Lambda$ -atom with mass  $m$  and internal levels  $|i\rangle$ ,  $i = 1, 2, 3$ , where  $|1\rangle$  and  $|2\rangle$  are

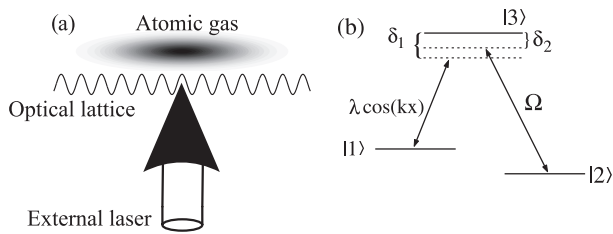


FIG. 1: Schematic configuration of system setup (a) and atom-laser configuration (b). The optical lattice drives the  $|1\rangle \leftrightarrow |3\rangle$  atomic transition and the external laser the  $|2\rangle \leftrightarrow |3\rangle$  transition.

the two lower metastable states and  $|3\rangle$  is the excited state. The atom moves in the presence of a one dimensional optical lattice which couples the two atomic states 1 and 3 with an effective coupling  $\lambda$ . The states 2 and 3 are coupled with an “external” field with amplitude  $\Omega$ , which is furthermore assumed constant over the extent of the atomic sample. Figure 1 details the system setup and laser-atom configuration we envision. Center-of-mass position and momentum are given by  $\hat{x}$  and  $\hat{p}$  respectively. Both atomic transitions are presumed highly detuned, with detunings  $\delta_1$  and  $\delta_2$  respectively, such that the excited state  $|3\rangle$  can be adiabatically eliminated resulting in an effective two-level model of the internal states  $|1\rangle$  and  $|2\rangle$ . Following standard procedures [16], we derive the effective Hamiltonian

$$\hat{H}_{sp} = \frac{\hat{p}^2}{2m} + \frac{\hbar\tilde{\Delta}}{2}\hat{\sigma}_z - \hbar\tilde{U}_1 \cos(2k\hat{x})\hat{\sigma}_{11} + \hbar\tilde{U} \cos(k\hat{x})\hat{\sigma}_x, \quad (1)$$

where  $\tilde{\Delta} = |\delta_1 - \delta_2| - \Omega^2/\delta_2 - \lambda^2/2\delta_1$  is an effective detuning taking into account for the constant Stark shifts of states 1 and 2,  $\tilde{U}_1 = \lambda^2/2\delta_1$ ,  $\tilde{U} = \lambda\Omega(1/2\delta_1 + 1/2\delta_2)$ ,  $k$  is the wave number of the optical lattice and for the  $\sigma$ -operators we have  $\hat{\sigma}_z = |2\rangle\langle 2| - |1\rangle\langle 1|$ ,  $\hat{\sigma}_x = |1\rangle\langle 2| + |2\rangle\langle 1|$  and  $\hat{\sigma}_{22} = |2\rangle\langle 2|$ . Note that the amplitudes  $\tilde{\Delta}$ ,  $\tilde{U}_1$  and  $\tilde{U}$  of the last three terms of (1) can be tuned independently within the validity regime of the adiabatic elimination. In the following we will use dimensionless parameters for brevity. Letting  $k^{-1}$  and  $E_r = \frac{\hbar^2 k^2}{2m}$  set characteristic length and energy scales we scale the variables as

$$\hat{x} = k\hat{x}, \quad \Delta = \frac{\hbar\tilde{\Delta}}{E_r}, \quad U_1 = \frac{\hbar\tilde{U}_1}{E_r}, \quad U = \frac{\hbar\tilde{U}}{E_r}. \quad (2)$$

In the  $|1\rangle = \begin{bmatrix} 0 \\ 1 \end{bmatrix}$  and  $|2\rangle = \begin{bmatrix} 1 \\ 0 \end{bmatrix}$  nomenclature, Eq. (1) becomes in scaled variables

$$\hat{H}_{sp} = -\frac{\partial^2}{\partial x^2} + \begin{bmatrix} \frac{\Delta}{2} & U \cos(\hat{x}) \\ U \cos(\hat{x}) & -\frac{\Delta}{2} - U_1 \cos(2\hat{x}) \end{bmatrix}. \quad (3)$$

The Hamiltonian (3) is periodic with period  $\lambda = 2\pi$  and thus, the operator  $\hat{T} = e^{\pm i\lambda\hat{p}}$  is a constant of motion. Moreover, the simultaneous inversion-displacement

operator

$$\hat{I} = \hat{\sigma}_z e^{\pm i\frac{\lambda}{2}\hat{p}} \quad (4)$$

defines another symmetry of the Hamiltonian where we explicitly have  $\hat{I}^2 = \hat{T}$  [17]. This additional invariant reveals that the spectrum is most properly described within a Brillouin zone where the quasi momenta extend between  $-1$  and  $1$ , despite the  $2\pi$  periodicity of the Hamiltonian. This property has been discussed in greater detail in Refs. [15, 17].

## B. Spectrum

Labeling the momentum eigenstates by  $|q\rangle$  ( $\hat{p}|q\rangle = q|q\rangle$ ), it is appropriate to divide the *bare basis states* into two sets

$$|\varphi_\eta(q)\rangle = \begin{cases} |q+\eta\rangle|1\rangle & \eta \text{ even} \\ |q+\eta\rangle|2\rangle & \eta \text{ odd} \end{cases} \quad (5)$$

$$|\phi_\eta(q)\rangle = \begin{cases} |q+\eta\rangle|2\rangle & \eta \text{ even} \\ |q+\eta\rangle|1\rangle & \eta \text{ odd}, \end{cases}$$

where  $\eta$  is any integer and  $q \in (-1, 1]$ . The Hamiltonian (3) is on block-diagonal form within these states and consequently does not couple basis states of different sets;  $\langle\varphi_{\eta'}(q')|\hat{H}|\phi_\eta(q)\rangle = 0$ . The analysis of Ref. [15] was carried out by taking into account for the possibility of populating both sets (5) simultaneously. Here we restrict ourself to one of the blocks of the Hamiltonian, namely discard the states  $|\phi_\eta(q)\rangle$ . Physically this implies that we assume a particular initial state of the atom. More precisely, assuming the atom to be ultracold with a momentum within the lowest Bloch band and initial internal state  $|1\rangle$ . Such a constrain on the initial atomic state seems reasonable within experimental feasibility. We point out though, by limiting our investigation to a single set of (5) we do not overlook any physical phenomena. One important observation is that scattering between atoms may cause the two sets of basis states  $|\varphi_\eta(q)\rangle$  and  $|\phi_\eta(q)\rangle$  to become coupled, even if they are disconnected by the Hamiltonian. We will return to this issue in Sec. IV B.

As a periodic problem, the eigenstates of  $\hat{H}$  will be on *Bloch form* imprinted with two quantum numbers, *band index*  $\nu = 1, 2, 3, \dots$  and quasi momentum  $q \in (-1, 1]$ ,

$$\hat{H}|\psi_\nu(q)\rangle = E^\nu(q)|\psi_\nu(q)\rangle, \quad (6)$$

where  $E^\nu(q)$  is the  $\nu$ 'th *Bloch band's* dispersion curve. Due to the coupled two-level structure, the dispersions may have anomalous shapes with multiple local minima [15, 17]. This should be compared to regular energy bands, by which we mean that either  $dE^\nu(q)/dq \geq 0$  or  $dE^\nu(q)/dq \leq 0$  for  $0 \leq q \leq 1$ . Figure 2 presents several examples of the first three bands. The atypical forms of the dispersions are clearly visible, and in [15] it was indeed demonstrated how such properties of the spectrum

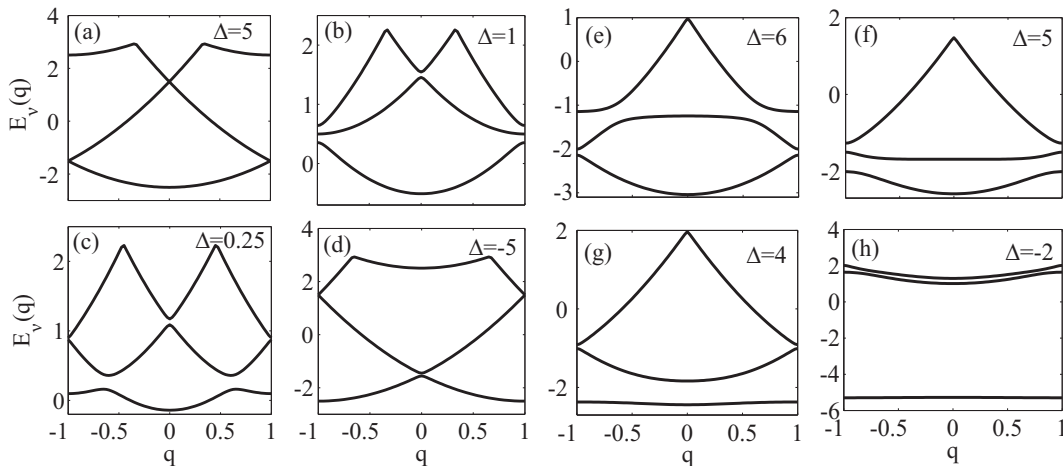


FIG. 2: Examples of the three lowest energy bands of Hamiltonian (3). In (a)-(d) we have  $U > U_1$  ( $U = 0.05$  and  $U_1 = 0.025$ ), while in (e)-(h)  $U < U_1$  ( $U = 0.1$  and  $U_1 = 2$ ). The multiple number of local minima of the lowest band is clear in (c). The large detuning case is shown in (a), in which the lowest band has the regular form.

renders a topological PT for fermions. Whenever  $U \gg U_1$  (plots (a)-(d)), situations similar to the ones presented in Ref. [15] are recovered. We remind that here, however, do we confine the spectrum to only one subset in Eq. (5). As was found in [15], the lowest dispersion curve can possess several local minima in this regime, which is shown in Fig. 2 (c). Note that for  $\Delta \gg 0$ , the regular spectrum for the lowest band is recovered, while for  $\Delta \ll 0$  is the spectrum "shifted" by one unit of momentum arising from the fact that we assumed the atoms to be initially in their internal state  $|1\rangle$ . The reverse is obtained by considering atoms initially in  $|2\rangle$  instead. Observe further that the excited bands in the plots for large detuning as well possess an irregular structure.

The situation is qualitatively different if instead  $\Delta, U_1 \gg U$ . Here, the internal states of the atoms are only weakly coupled and we can approximate the spectrum by consisting of free particles (atoms in internal state  $|2\rangle$ ) and atoms in a potential  $U_1 \cos(2x)$  (atoms in internal state  $|1\rangle$ ). The corresponding two spectrums may overlap forming unusual appearances. For large  $U_1$ , the lowest dispersion curves, corresponding to  $|1\rangle$ -atoms, are almost flat. Thus, slight non-zero repulsive interaction between the atoms in such a band would cause an insulating state. However, the size and sign of the detuning  $\Delta$  determines if the overall lowest band belongs to  $|1\rangle$  or  $|2\rangle$  atoms and therefore if the state is in a superfluid or a Mott state, provided repulsive atom-atom interaction. Thus, for long enough time periods for the system to relax to its thermal equilibrium state, it is possible to achieve a SF-Mott PT by changing the detuning. These conclusions are verified in Fig. 2 (e)-(h), where in (e) the lowest dispersion curve is approximately parabolic while in (h) it is almost flat. Similar structure of the dispersions, mixture of narrow and wide energy bands, was also encountered in honeycomb lattices [18].

### III. THE BOSE-HUBBARD HAMILTONIAN

One among the prototype models of many-body physics and the study of quantum PTs is the *Bose-Hubbard model* [19]. The dynamics is driven by two terms representing hopping between sites and on-site interaction between the particles. For ultracold bosonic atoms in optical lattices, the analysis is most often restricted to consider only the lowest band, *single band approximation*, and to hopping between neighboring sites, *tight binding approximation*. In this paper we as well impose these approximations, and the validity of such assumptions will be discussed in detail in Sec. IV C.

#### A. Second quantization

The many-body Hamiltonian is given by

$$\hat{H} = \int \hat{\Psi}^\dagger(x) \cdot \left\{ -\frac{d^2}{dx^2} + \begin{bmatrix} \frac{\Delta}{2} & U \cos(\hat{x}) \\ U \cos(\hat{x}) & -\frac{\Delta}{2} - U_1 \cos(2\hat{x}) \end{bmatrix} + \frac{1}{2} \hat{\Psi}^\dagger(x) \cdot \mathbf{g} \cdot \hat{\Psi}(x) \right\} \cdot \hat{\Psi}(x) dx, \quad (7)$$

where  $\hat{\Psi}(x)$  and  $\hat{\Psi}^\dagger(x)$  are atomic spinor annihilation and creation field operators respectively and

$$\mathbf{g} = \begin{bmatrix} g_{11} & g_{12} \\ g_{12} & g_{22} \end{bmatrix} \quad (8)$$

is the scaled onsite interaction matrix with amplitudes  $g_{ij}$ . We will make the approximation of assuming equal scattering amplitude between the internal condensate states  $|1\rangle$  and  $|2\rangle$ ,  $g_{11} = g_{22} = g$ , and letting  $g_{12} = 0$ . It

is believed that such an assumption modifies the onsite interaction term only slightly. The atomic field operators is conveniently expressed in terms of Wannier functions as

$$\hat{\Psi}(x) = \sum_i e^{i\theta_i} \mathbf{w}_i(x) \hat{b}_i, \quad (9)$$

where  $\mathbf{w}_i(x) = \mathbf{w}(x - x_i)$  is the lowest band's two-component Wannier function located at  $x_i$  and  $i$  runs over all lattice sites,  $\hat{b}_i$  is the bosonic annihilation operator for the lowest band at site  $i$  and the  $\theta_i$ 's are phases that will be determined later. Using (9), we derive the second quantized Hamiltonian

$$\begin{aligned} \hat{H}_{sb} = & - \sum_{i,j} J_{ij} \hat{b}_i^\dagger \hat{b}_j e^{i(\theta_j - \theta_i)} \\ & + \frac{1}{2} \sum_{ijkl} G_{ijkl} \hat{b}_i^\dagger \hat{b}_j^\dagger \hat{b}_k \hat{b}_l - \mu \sum_i \hat{n}_i. \end{aligned} \quad (10)$$

Here we have introduced the chemical potential  $\mu$ , and

$$J_{ij} = - \int \mathbf{w}_i^\dagger(x) \cdot \hat{H}_{sp} \cdot \mathbf{w}_j(x) dx, \quad (11)$$

$$G_{ijkl} = g \int \mathbf{w}_i^\dagger(x) \cdot (\mathbf{w}_j^\dagger(x) \cdot \mathbf{w}_k(x)) \cdot \mathbf{w}_l(x) dx$$

are the overlap integrals determining the strength of hopping and atom-atom interaction as function of the system parameters  $\Delta$ ,  $U_1$  and  $U$ . So far, no tight binding approximation has been applied. However, imposing the single band approximation normally motivates the use of the tight binding approximation [21], in which case one obtains the regular Bose-Hubbard Hamiltonian

$$\begin{aligned} \hat{H}_{BH} = & -J_1 \sum_{\langle i,j \rangle} \hat{b}_i^\dagger \hat{b}_j e^{i\theta_{ji}} \\ & + \frac{G_0}{2} \sum_i \hat{n}_i (\hat{n}_i - 1) - \mu \sum_i \hat{n}_i, \end{aligned} \quad (12)$$

where  $\theta_{ji} = \theta_j - \theta_i$ . The first sum runs over nearest neighbors, the coefficients  $J_1 \equiv J_{ii+1}$  and  $G_0 \equiv G_{iiii}$  and  $\hat{n}_i = \hat{b}_i^\dagger \hat{b}_i$ . The phases  $\theta_{li}$  are chosen such that the total energy is minimized, giving

$$\theta_{ji} = \begin{cases} 0, & J_1 > 0 \\ \pi, & J_1 < 0. \end{cases} \quad (13)$$

The position parameters  $x_i$  of the  $i$ 'th Wannier function are not *a priori* given in the present model. In general, the  $x_i$ 's are taken to coincide with the minima of the effective potential. Here, however, the coupled dynamics provide a situation where well defined potentials cannot be ascribed single internal atomic states. These issues were analyzed in more detail in [15] and it was in particular found that  $x_i = n\pi$  for any integer  $n$  renders

Wannier functions having the familiar shapes, which for a deep lattice approximate the harmonic oscillator eigenstates. This finding may be motivated by the following argument. For positive detuning and  $\Delta \gg U \gg U_1$ , the lowest dispersion has the regular form (see Fig. 2 (a)), and since the initial atomic states are chosen to be  $|1\rangle$  the effective lattice potential is in this case  $U_{eff}(x) \propto \cos^2(x)$  which possesses its minima for  $x_i = n\pi$ . Assuming a deep lattice, the Wannier functions then attains, to a good accuracy, the forms of the corresponding harmonic oscillator eigenfunctions in this limit. We have found that the Wannier functions preserve their typical forms even for decreasing detunings  $\Delta$  if we pick  $x_i = n\pi$ . This is indeed only true for  $x_i = n\pi$  once we have restricted the analysis to the basis set  $|\varphi_\eta(q)\rangle$  of Eq. (5). Therefore, in the following we will choose  $x_i = n\pi$ .

Let us comment on the elaborate structure of the system. For large detunings,  $|\delta_1| \gg \lambda$  and  $|\Delta| \gg \lambda, \Omega$ , atoms in state  $|1\rangle$  moves in an effective potential  $U_{eff}(x) \propto \cos^2(x)$ . This is the common dispersive situation utilized in most experiments. The effective potential is obtained via adiabatic diagonalization of the Hamiltonian. It is known that such approach gives rise to non-adiabatic corrections, which can be expressed in terms of effective gauge fields [22]. However, in the dispersive regime, the gauge fields are vanishingly small and can be neglected. In the intermediate regime, which we are interested in, on the other hand, the non-adiabatic corrections cannot be overlooked and must be taken into account. In fact, only in the limiting situations  $|\Delta| \rightarrow \infty, 0$  can an effective potential be assigned to the internal states of the atoms [15].

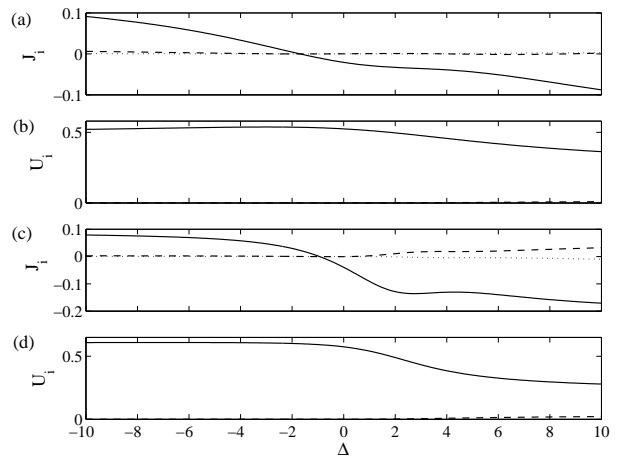


FIG. 3: Two examples of the first three hopping parameters  $J_1$  (solid line),  $J_2$  (dashed line) and  $J_3$  (dotted line) as function of  $\Delta$  in (a) and (c), and  $G_0$  (solid line) and  $G_1$  (dashed line) in (b) and (d). In both examples,  $J_1$  change sign. The dimensionless parameters are  $U = 1$  and  $U_1 = 0.5$  in (a) and (b), and  $U = 0.5$  and  $U_1 = 1$  in (c) and (d).

## B. Coupling parameters

The anomalous form of the lowest dispersion curve implies that the nearest neighbor hopping parameter  $J_1$  can attain both positive and negative values [12]. The coupling parameters, given by the various overlap integrals (11), are calculated using the Wannier functions obtained numerically from diagonalization of the Hamiltonian (3). We display, as a function of  $\Delta$ ,  $J_i$  ( $i = 1, 2, 3$ ) in Fig. 3 (a) and (c), while (b) and (d) show  $G$  and  $G_1$ , where  $G_1 = G_{ijji}$  and  $j = i \pm 1$ . The parameters  $J_2 \equiv J_{ii+2}$  and  $J_3 \equiv J_{ii+3}$  describe the next and next-next nearest neighbor tunneling strengths. The parameters are  $U = 1$  and  $U_1 = 0.5$  in (a) and (b), and  $U = 0.5$  and  $U_1 = 1$  in (c) and (d). In these two examples  $|J_1| \gg |J_{i \neq 1}|$  outside the neighborhood where  $J_1 = 0$ . This is, however, not necessarily always the case for other choices of parameters. We note that  $G_1$  is considerably smaller than  $G_0$  for any  $\Delta$ .

## IV. MOTT-SUPERFLUID PHASES

In the previous section we found that the hopping coefficient may change sign as  $\Delta$  is varied. Thus, the effective hopping,  $J_1/G_0$ , can be tuned from large negative to large positive values. The character of the many-body atomic state is different depending on the sign of  $J_1$  which comes about because of the phase matching between the Wannier functions in the expansion (9). We will demonstrate in Sec. IV, that ballistic expansion of the atomic state renders dissimilar interference patterns depending on the phase  $\theta$ .

For the phase diagrams, this implies that both positive and negative regimes for the hopping should be considered, and not just positive as in the regular Bose-Hubbard model [19]. We will present typical examples of the phase diagrams in the  $\mu - \Delta$  plane rather than in the  $\mu - J_1$  plane, since experimentally  $\Delta$  is an easily controllable parameter. The phase diagrams are achieved by applying the *strong coupling expansion* [20], which has turned out to reproduce accurate results for the Mott boundaries of the BH model in one dimension.

### A. Modified strong coupling expansion

We first recapitulate the general idea behind the strong coupling expansion approach [20]. In general, the Mott insulating state is obtained in the regime where onsite interaction dominates the tunneling,  $G_0 > J_1$ . Thus, an expansion in the parameter  $J_1/G_0$  is likely to yield a proper phase diagram for the Mott lobes. In one dimension, the method has indeed been shown to agree well with more sophisticated Monte Carlo approaches [20].

In lowest order (infinitely deep lattice), the first term of the Hamiltonian (12) is neglected and the model is

diagonal in the Fock basis. Degenerate perturbation theory applied to the first term is then performed to third order in the parameter  $J_1/G_0$ . In particular, we derive the energy  $E_M(n_0)$  for a Mott state with exactly  $n_0$  particles per site and the energies  $E_{\pm}(n_0)$  for the superfluid states with one particle added or subtracted from the Mott state. These energies will depend on the system parameters and especially on the re-scaled chemical potential  $\bar{\mu} = \mu/G_0$ . The solutions, in terms of  $\bar{\mu}$ , of the equations

$$\begin{aligned} E_{+1}(n_0) - E_M(n_0) &= 0, \\ E_{-1}(n_0) - E_M(n_0) &= 0 \end{aligned} \quad (14)$$

determines the Mott boundaries. The conditions (14) give the upper and lower Mott boundaries  $\bar{\mu}_+(n_0)$  and  $\bar{\mu}_-(n_0)$  respectively, and the  $n_0$ 'th Mott zone is defined by  $\bar{\mu}_+(n_0) > \bar{\mu}_-(n_0)$ . The outcome of a third order perturbation theory, first presented in [20], read

$$\begin{aligned} \bar{\mu}_+(n_0) &= n_0 + 1 - 2t(n_0 + 1) + t^2 n_0^2 \\ &\quad + t^3 n_0(n_0 + 1)(n_0 + 2), \\ \bar{\mu}_-(n_0) &= n_0 + 2tn_0 - t^2(n_0 + 1)^2 \\ &\quad + t^3 n_0(n_0 + 1)(n_0 - 2), \end{aligned} \quad (15)$$

where,  $t = |J_1|/G_0$ .

### B. Phase diagrams

The Mott boundaries for  $n_0$  particles per site, as given in Eq. (15), depend on  $t$ . The parameter  $t$ , on the other hand, have a complex dependence of the experimentally attainable quantities  $\Delta$ ,  $U$  and  $U_1$ . To study the crossover between positive and negative hopping  $J_1$ , we saw in the previous section that by sweeping the detuning  $\Delta$  such a situation is often encountered. The phase diagrams will therefore be analyzed in the  $\bar{\mu} - \Delta$  plane, keeping  $U$  and  $U_1$  fixed. We derive  $t$  from the numerically obtained Wannier functions. The parameters  $U$  and  $U_1$  are chosen in such a way that we can impose the above approximations (see also the following subsection).

The phase diagrams obtained for the parameters of Fig. 3 (a) and (c) are displayed in Fig. 4 (a) and (b) respectively. We only show the first four Mott lobes. The vertical dashed line shows the crossover between positive and negative  $J_1$ ; left of the line  $J_1 > 0$  and right of it  $J_1 < 0$ . We note the asymmetry of the Mott zones on each side of the dashed line. This irregularity originates from the Stark shift term  $U_1 \cos(2x)$  (only affecting atoms in state  $|1\rangle$ ) in the Hamiltonian (3). Without this term [23], the Mott lobes are symmetric with respect to the dashed line. Moreover, the dashed line are at  $\Delta = 0$  in such a case ( $U_1 = 0$ ), which can be understood since this term renders an effective detuning term and hence shift the resonance condition  $\Delta = 0$ .

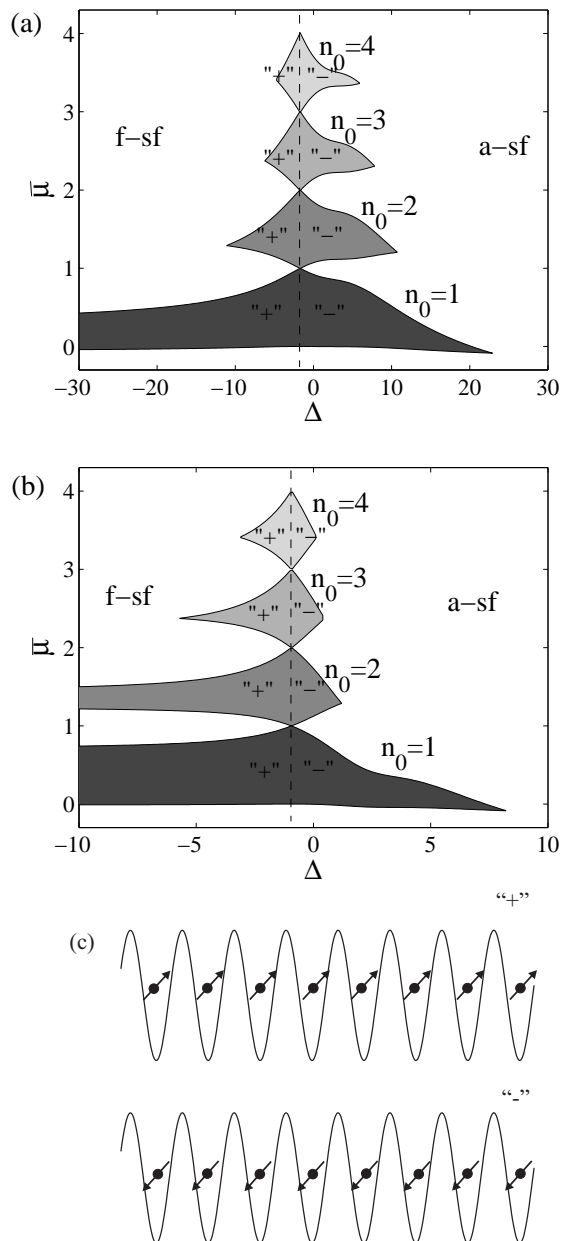


FIG. 4: Upper two plots (a) and (b) display the phase diagrams (showing the first four Mott lobes) corresponding to Fig. 3 (a) and (c). The vertical dashed lines is the phase boundary between antiferromagnetic (a-sf) or ferromagnetic superfluid states (f-sf) and between “+” and “-” Mott phases. The lower plot (c) gives a schematic picture of the “+” and “-” Mott states.

In Ref. [15], we demonstrated that a PT is obtained in an ideal gas of coupled two-component atoms in an optical lattice, when the detuning is varied across a critical value. In the case of fermions, this describes a topological PT, as the fermi surface changes topology across the critical point; each atom changes its momenta by either

$\pm 1$ . The nature of such a PT was addressed in Ref. [15], and in particular it was found to be first order. Changing the internal states of the atoms also shift the atomic momenta by a multiple of the unit momentum. This yields a competition between the two terms; for certain parameters is it more favorable to lower the internal atomic energies, while in other situations the atomic kinetic energy should be minimized. Crossing the critical point for this PT, which occurs exactly when the hopping changes sign, each atom shift their momenta by  $\pm 1$  and their internal states are swapped. Thus, the collective atomic inversion, which gives the population imbalance between the internal atomic states, works as an order parameter [15]. Representing the internal atomic state as a spin 1/2 particle, we schematically show the significance of the “+” Mott and the “-” Mott states in Fig. 4 (c).

The same type of PT exists also for incommensurate filling (superfluid state). However, contrary to atoms in the Mott state, the superfluid states possess a coherence between the atoms and this PT manifests itself in this coherence as well. In particular, such transition corresponds to going from an antiferromagnetic (a-sf) to a ferromagnetic superfluid state (f-sf), or vice versa. The terms antiferro- and ferromagnetic come from phase matching between site wave functions in the expansion (9). For the antiferromagnetic state, there is a  $\pi$ -phase sign-flip between neighboring Wannier functions.

The analysis has been carried out by restricting the atomic states to the set  $\{|\varphi_\eta(q)\rangle\}$  of Eq. (5). Already pointed out, atom-atom scattering may induce coupling between the sets of (5). Indeed, we have verified that such coupling terms have non-negligible coefficients. However, the characteristics are identical between the two sets. That is, varying the system parameters, atoms receding in the  $\{|\varphi_\eta(q)\rangle\}$  set undergo the same dynamics as atoms of the  $\{|\phi_\eta(q)\rangle\}$  set. Apart from an overall shift of momenta, the spectrums are the same for the two sets and consequently also the phase diagrams. Therefore, for weak atom-atom interaction, our conclusions are not changed by including scattering between the two sets.

### C. Validity of approximations

Various approximations have been imposed in order to derive the phase diagrams; tight binding and single band approximations, and truncating the strong coupling expansion at third order. In this subsection we systematically discuss the justification of such assumptions. A rule of thumb is that these approximations are all related in the regular Bose-Hubbard model and share more or less the same validity regimes [21].

Already Fig. 2 indicates the justification of only consider nearest neighbor and onsite interaction. Other terms arising from a Wannier expansion and second quantization of the Hamiltonian (not included in Fig. 2) have been verified to be very small in the parameter regimes that we study. Concerning hopping beyond near-

est neighbors, we have modified the strong coupling expansion to include such processes and recalculated the phase diagrams of Fig. 4 and found only minimal corrections. Thus, the quantitative structure of the phase diagrams remain even when hopping to next-nearest, next-next-nearest neighbors and so on are taken into account. Note that when  $J_1 = 0$  the tight binding approximation in general fails. In this regime, however, the hopping terms beyond nearest neighbor are, for the examples presented in this paper, very small such that the dynamics is predominantly driven by the onsite interaction and therefore the system must be in a Mott state.

The condition for application of the single band approximation may be investigated by evaluating overlap integrals between Wannier functions of the first and the second band

$$L_{ij} = \int dx \mathbf{w}_i(x) \cdot \hat{H}_{sp} \cdot \mathbf{w}_j(x), \quad (16)$$

where  $\mathbf{w}_j(x)$  is the spinor Wannier function corresponding to the second band at site  $j$ . It turns out that onsite integrals dominate,  $i = j$ . For Fig. 4, we have  $L_{ii} \ll J_1, G_0$  everywhere except for  $\Delta \approx 0$  in (b). Thus, tuning  $\Delta$  non-adiabatically across resonance, when  $U = 0.5$  and  $U_1 = 1$ , may cause population of excited bands.

Finally, we also discuss on what grounds the third order strong coupling expansion may be applied. For the regular Bose-Hubbard Hamiltonian it is well known that the approach accurately reproduce the Mott-zones [20]. From (15) it follows that the  $k$ 'th order term in the expansion scales as  $n_0^k$  for large  $n_0$ . Thus, for a proper description of the higher Mott zones must  $tn_0 < 0$  within the Mott. This is true for the regular Bose-Hubbard model, where the extension of the Motts decrease roughly as  $n_0^{-1}$  [21]. From Fig. 4, this is indeed found to be true also for the current model using the spinor Wannier functions. We have compared the phase diagrams of Fig. 4 with the ones obtained by utilizing second order perturbation theory instead of third order and found only slight modifications.

## V. CHARACTER OF DIFFERENT PHASES

As pointed out in the introduction, coupled two-level atoms in optical lattices was first considered in Ref. [12], considering two optical lattices driving a Raman transition in  $\Lambda$  atoms. Tuning the relative phase between the two lattices, it was demonstrated that the hopping coefficient in the corresponding Bose-Hubbard Hamiltonian could attain negative as well as positive values. Furthermore, due to the phase factor in the Wannier expansion (9), it follows that the coherence in a superfluid state is different depending on the sign of the hopping coefficient. In particular, if the phase difference between consecutive Wannier functions in (9) is  $\pi$  the superfluid state was termed *antiferromagnetic*, while a zero phase difference

characterizes *ferromagnetic* superfluid states. It was also predicted that ballistic expansion of an antiferromagnetic or ferromagnetic superfluid state would render dissimilar time-of-flight measurements. In this section we will analyze the corresponding scenario in the model we consider.

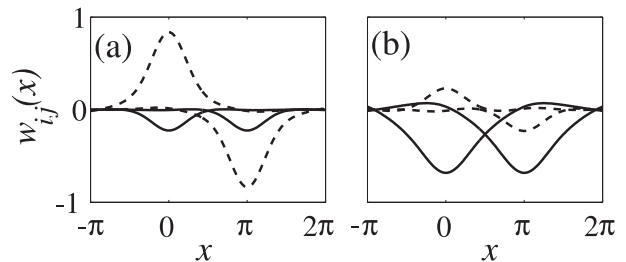


FIG. 5: Neighboring constituent Wannier functions  $w_{j,1}(x)$  (dotted) and  $w_{j,2}(x)$  (solid). In (a)  $J_1 \approx 0.1$  corresponding to  $U = 1$ ,  $U_1 = 0.5$ ,  $\Delta = -11.5$ , while  $J_1 \approx -0.1$  in (b) obtained by choosing  $U = 1$ ,  $U_1 = 0.5$ ,  $\Delta = 11.5$ . Note that the dashed but not the solid line flip phase between neighboring sites.

### A. Effect of positive and negative hopping coefficients

In the internal  $\{|1\rangle, |2\rangle\}$  basis, the spinor Wannier function at site  $i$  is decomposed as

$$\mathbf{w}_j(x) = \begin{bmatrix} w_{j,1}(x) \\ w_{j,2}(x) \end{bmatrix}. \quad (17)$$

For situation lacking internal structure, we have for neighboring Wannier functions,  $w_j(x) = e^{i\varphi} w_{j+1}(x)$  for some phase  $\varphi$ . This is not the case for the spinor Wannier function  $\mathbf{w}_j(x)$  of Eq. (17). However, it is true for its constituent parts. In particular, for the lowest band we find real Wannier functions satisfying  $w_{j,1}(x) = -w_{j+1,1}(x)$  and  $w_{j,2}(x) = w_{j+1,2}(x)$ . This is visualized in Fig. 5 showing two examples of the neighboring Wannier functions. In (a), the nearest neighbor tunneling coefficient is positive,  $J_1 \approx 0.1$ , while in (b) it is negative but with the same amplitude,  $J_1 \approx -0.1$ . The internal probabilities for a given Wannier functions is roughly interchanged between the two examples of Fig. 5, which follows from the sign flip of the detuning  $\Delta$  between (a) and (b). This is indeed also related to the PT discussed in the previous section and in [15], where an abrupt jump in the collective atomic inversion is seen when crossing the critical point. Thus, a state selective measurement distinguishes between antiferromagnetic or ferromagnetic states and between Mott “+” and Mott “-” states. In the next subsection, we also show how a time-of-flight detection can separate between the different superfluid states.

## B. Time-of-flight detection

As predicted in [12], the two superfluid states may be recognized via a time-of-flight measurement of an freely expanding gas of atoms, which will be shown in this Sub-section.

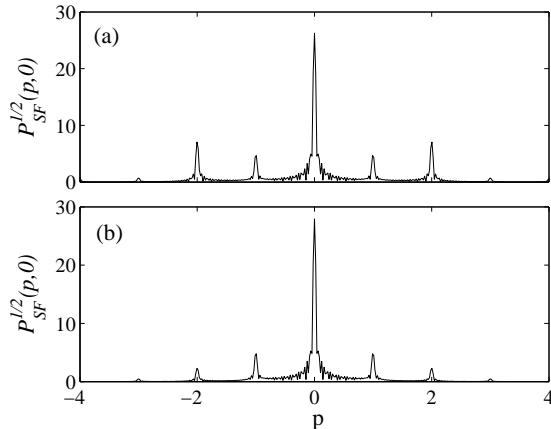


FIG. 6: The momentum distributions of the state (18) with  $\Delta = -11.5$  (a) and  $\Delta = 11.5$  (b). The other dimensionless parameters are as in Fig. 5. The peaks at  $p = \pm 2$  are more pronounced in (a) than in (b) giving different interference patterns of the freely expanding atomic condensates.

Our idea is to study the different interferences induced by having 0 or  $\pi$  phase correlation between neighboring sites. Thus, we have a matter wave function as

$$\Psi_{SF}(x, 0) = \sum_j e^{i\theta_j} \begin{bmatrix} w_{j1}(x) \\ w_{j2}(x) \end{bmatrix} \quad (18)$$

and study the impact of having

$$\theta_j = \begin{cases} 0, & J_1 > 0 \\ j\pi, & J_1 < 0 \end{cases} \quad (19)$$

when the wave function is freely evolving. The ballistically expanded wave function reads

$$\Psi_{SF}(x, t_{tof}) = e^{-i\hat{p}^2 t_{tof}} \Psi_{SF}(x), \quad (20)$$

where  $t_{tof}$  is the time-of-flight time between release of the superfluid state till measurement of it. The total probability distribution

$$P_{tot}(x, t_{tof}) = |\Psi_{SF}(x, t_{tof})|^2 \quad (21)$$

or the constituent probability distributions  $P_i(x, t_{tof})$  ( $i = 1, 2$ ) for the atomic internal states are assumed detected after the ballistic expansion. For  $t_{tof} \rightarrow \infty$ , the momentum distribution  $P_{SF}(p, t = 0)$  corresponding to  $\Psi_{SF}(x, 0)$  in Eq. (18), is encoded into the distribution  $\Psi_{SF}(x, t_{tof} = \infty)$ . In Fig. 6, we display the square root

of the momentum distributions of  $\Psi_{SF}(x, 0)$ . In (a) we use the parameters of Fig. 5 (a) (and thus a constant phase between the Wannier functions), while in (b) the parameters are as in Fig. 5 (b) ( $\pi$  phase modulation between the neighboring Wannier functions). For  $J_1 > 0$ , the even numbers of momenta are more strongly populated; the peaks around  $\pm 2$  are more distinct in Fig. 6 (a) than in (b). Note that for this example  $J_1$  have the same strength in both cases, but the corresponding Wannier functions (see Fig. 5) are different. Thus, it is not only the phase  $\theta_j$  which distinguishes the two cases.

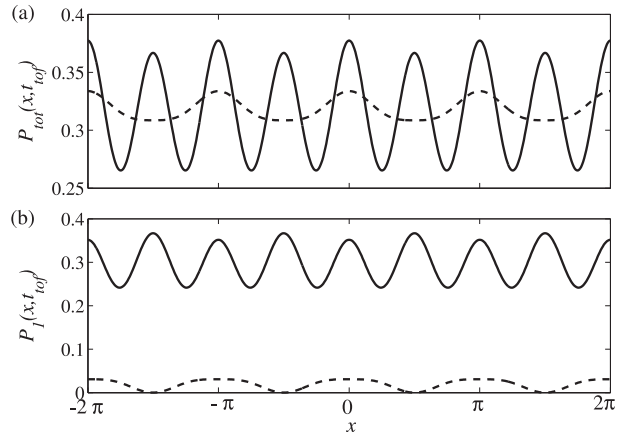


FIG. 7: Atomic distributions  $P_{tot}(x, t_{tof})$  (a) and  $P_1(x, t_{tof})$  (b) after a time-of-flight spreading  $t_{tof} = 4$ . For solid lines;  $\Delta = 11.5$ , while for dotted lines;  $\Delta = -11.5$ , and in both cases  $U = 1$  and  $U_1 = 0.5$ . This set of parameters give  $J_1 = 0.1$  and  $J_1 = -0.1$  respectively. The difference between solid and dotted lines derives from the different Wannier functions of the two cases, but also from the phase factor  $e^{i\theta_j}$  in the Wannier expansion (9).

The difference in momentum distributions will also manifest itself in the position distributions  $P_{tot}(x, t_{tof})$  and  $P_i(x, t_{tof})$  for finite times  $t_{tof}$ . The results for the total probability distribution (21) and the distribution for the internal state 1,  $P_1(x, t_{tof})$ , are depicted in Fig. 7 (a) and (b) respectively. The time-of-flight  $t_{tof} = 4$ , guaranteeing that the interference has been well established. Noticeable from the figure is that for positive hopping the distribution shows a super-structure with two local maxima for each period, not seen for  $J_1 < 0$ . The great difference in probability amplitude between the internal atomic states in (b) derives from the fact that two internal states are unequally populated due to the different detunings;  $\Delta = 11.5$  and  $\Delta = -11.5$ .

## VI. CONCLUSIONS

In this work we have presented an *ab initio* analysis of a gas of coupled two-level atoms in an optical lattice. The spectrum of the single particle Hamiltonian was found to possess peculiar characteristics originating from the



coupled dynamics. In particular, the hopping amplitude describing tunneling between nearest sites in the optical lattice can attain positive as well as negative values. In an earlier work, we demonstrated that PTs can be obtained in the current model in the absence of atom-atom interaction [15]. Including scattering between the atoms, as in this paper, we identified the PT of Ref. [15] as the sign change in the hopping parameter. The corresponding PT was shown to be between antiferromagnetic and ferromagnetic superfluid states, or between distinguishable Mott states. Moreover, a thorough analysis about the effect of a positive or a negative nearest neighbor tunneling coefficient was given, focusing on time-of-flight detection of the condensate. The model is readily generalized to two and three dimensions [15], and the phase diagrams would show similar structures.

The imposed approximations and their validity regimes were studied. The present paper restricts the analysis to regimes where these approximations are justified. However, it is expected that new phenomena will occur be-

yond such limitations. For example, the nearest neighbor hopping may vanish, and consequently long range or semi-long range interaction might become important. Here, however, the parameters were chosen such that whenever  $J_1 = 0$ , also hopping beyond nearest neighbors could be neglected,  $J_i \approx 0$   $i = 2, 3, \dots$  in comparison to the onsite interaction. The reason for this choice was to remain within the validity of our approximations. We are currently investigating regimes outside single band and tight binding approximations by using different methods. These results are left for future publications. We are also studying the dynamics of the condensate as the system is driven through the critical point  $J_1 = 0$ .

### Acknowledgments

JL acknowledges support from the MEC program (FIS2005-04627).

- 
- [1] M. Lewenstein, A. Sanpera, V. Ahufinger, B. Damski, A. Sen, and U. Sen, *Adv. Phys.* **56**, 243 (2007).
- [2] M. Greiner, O. Mandel, T. Esslinger, T. W. Hänsch, and I. Bloch, *Nature* **415**, 39 (2002).
- [3] B. Juliette, V. Josse, Z. Zuo, A. Bernard, B. Hambrecht, P. Lugan, D. Clément, L. Sanchez-Palencia, P. Bouyer, and A. Aspect, *Nature* **453**, 891 (2008); G. Roati, C. D’Errico, L. Fallani, M. Fattori, C. Fort, M. Zaccanti, G. Modugno, and M. Inguscio, *Nature* **453**, 895 (2008).
- [4] B. Parades, A. Widera, V. Murg, O. Mandel, S. Fölling, I. Cirac, G. V. Schlyapnikov, T. W. Hänsch, and I. Bloch, *Nature* **429**, 277 (2004).
- [5] U. Schneider, L. Hackermüller, S. Will, I. Bloch, T. A. Costi, R. W. Helmes, D. Rasch, and A. Rosch, arXiv:0809.1464.
- [6] E. Demler, and F. Zhou, *Phys. Rev. Lett.* **88**, 163001 (2002); A. Imambekov, M. Lukin, and E. Demler, *Phys. Rev. A* **68**, 063602 (2003); J. J. Garcia-Ripoll, M. A. Martin-Delgado, and J. I. Cirac, *Phys. Rev. Lett.* **93**, 250405 (2005); T. Kimura, S. Tsuchiya, and S. Kurihara, *Phys. Rev. Lett.* **94**, 110403 (2005); R. V. Pai, K. Sheshadri, and R. Pandit, *Phys. Rev. B* **77**, 014503 (2008).
- [7] O. Mandel, M. Greiner, A. Widera, T. Rom, T. W. Hänsch, and I. Bloch, *Phys. Rev. Lett.* **91**, 010407 (2003).
- [8] M. S. Chang, C. D. Hamley, M. D. Barrett, J. A. Sauer, K. M. Fortier, W. Zhang, L. You, and M. S. Chapman, *Phys. Rev. Lett.* **92**, 140403 (2004).
- [9] D. M. Stamper-Kurn, H. J. Miesner, A. P. Chikkatur, S. Inouye, J. Stenger, and W. Ketterle, *Phys. Rev. Lett.* **83**, 661 (1999).
- [10] L. E. Sadler, J. M. Higbie, S. R. Leslie, M. Vengalattore, and D. M. Stamper-Kurn DM, *Nature* **443**, 312 (2006).
- [11] A. Albus, A. Alluminati, and J. Eisert, *Phys. Rev. A* **68**, 023606 (2003); H. P. Buchler, and G. Blatter, *Phys. Rev. Lett.* **91**, 130404 (2003); M. Lewenstein, L. Santos, M. A. Baranov, and H. Fehrmann, *Phys. Rev. Lett.* **92**, 050401 (2004); K. Gunter, T. Stoferle, H. Moritz, M. Köhl, and T. Esslinger, *Phys. Rev. Lett.* **96**, 180402 (2006).
- [12] K. V. Kuritsky and R. Graham, *Phys. Rev. Lett.* **91**, 240406 (2003).
- [13] K. V. Kuritsky and R. Graham, *Phys. Rev. A* **70**, 063610 (2004); K. V. Kuritsky, M. Timmer, and R. Graham, *Phys. Rev. A* **71**, 033623 (2005).
- [14] J. J. Garcia-Ripoll and J. K. Pachos, *New J. Phys.* **9**, 139 (2007); M. Eckholt and J. J. Garcia-Ripoll, *Phys. Rev. A* **77**, 063603 (2008).
- [15] J. Larson and J.-P. Martikainen, To appear in *Phys. Rev. A*, arXiv:0808.3891.
- [16] M. Alexanian and S. K. Bose, *Phys. Rev. A* **52**, 2218 (1995).
- [17] W. Ren and H. J. Carmichael, *Phys. Rev. A* **51**, 752 (1995); J. Larson, J. Salo, and S. Stenholm, *Phys. Rev. A* **72**, 013814 (2005).
- [18] C. Wu and D. S. Sarma, *Phys. Rev. B* **77**, 174509 (2008).
- [19] M. P. A. Fisher, P. B. Weichman, G. Grinstein, and D. S. Fisher, *Phys. Rev. B* **40**, 546 (1989); S. Sachdev, *Quantum Phase Transitions*, (Cambridge University Press, 2006).
- [20] J. K. Freericks and H. Monien, *Europhys. Lett.* **26**, 545 (1994).
- [21] J. Larson, S. Fernández-Vidal, G. Morigi, and M. Lewenstein, *New J. Phys.* **10**, 045002 (2008).
- [22] C. A. Maed, *Rev. Mod. Phys.* **64**, 51 (1992); A. Bohm, A. Mustafazadeh, H. Kuizumi, Q. Niu, and J. W. Zwanziger, *Geometrical Phase in Quantum Systems*, (Springer, Berlin, 2003).
- [23] Discarding this term from the Hamiltonian gives a model in which the two atomic states are directly coupled by the optical lattice, see [15].